Research Square

Preprints are preliminary reports that have not undergone peer review.
They should not be considered conclusive, used to inform clinical practice,
or referenced by the media as validated information.

Agulhas Current Variability and Ocean Heat Transport Implications for Regional Climate Variability and Extreme Ocean Conditions

Krishna K. M

munikrishnna@yahoo.co.in

Andhra University

B. Usha Rani

Andhra University

Research Article

Keywords: Agulhas Current, Western Boundary Current Dynamics, Volume Transport Variability, Ocean Heat Transport, Interannual Variability, Indian Ocean Dipole, ENSO, Wind Stress Curl

Posted Date: November 13th, 2026

DOI: https://doi.org/10.21203/rs.3.rs-11162110/v1

License: This work is licensed under a Creative Commons Attribution 4.0 International License.
Read Full License

Additional Declarations: No competing interests reported.

Agulhas Current Variability and Ocean Heat Transport Implications for Regional Climate Variability and Extreme Ocean Conditions

Krishna K.M[a*] and B. Usha Rani[b]

[a]Krishna: ORCID®0000-0002-2629-7530

[a,b]Department of Meteorology and Oceanography, College of Science and Technology, Andhra University, Visakhapatnam, INDIA

Corresponding author: Krishna K.M[*], E-mail: munikrishnna@yahoo.co.in

Abstract

The Agulhas Current is one of the strongest western boundary currents of the global ocean and plays a fundamental role in the exchange of heat and salt between the Indian and Atlantic Oceans through the Agulhas leakage system. Variability in the current influences regional circulation, inter-basin exchange, and potentially the Atlantic Meridional Overturning Circulation (AMOC). Despite its climatic importance, the relative roles of atmospheric forcing, large-scale climate variability, and intrinsic ocean dynamics in controlling Agulhas Current transport remain incompletely understood. This study investigates the mean structure, transport variability, heat transport characteristics, and forcing mechanisms of the Agulhas Current using an Eulerian framework based on ocean reanalysis and atmospheric datasets.

The mean circulation is characterized by a narrow, surface-intensified western boundary current extending to depths of approximately 800–1000 m, followed by a pronounced retroflection south of Africa. Volume transport estimates reveal a persistent southward flow with a mean transport of approximately 63 Sv and substantial variability (standard deviation ≈ 21 Sv), indicating a highly dynamic current system. Spectral and time-series analyses show that variability is dominated by interannual and longer-timescale fluctuations, with only weak seasonal modulation and no significant long-term trend. Comparison with the Niño-3.4 and Dipole Mode Index (DMI) indicates episodic correspondence with ENSO and Indian Ocean Dipole variability, but no robust or consistent relationship.

Heat transport diagnostics demonstrate that the Agulhas Current is a major pathway for poleward heat redistribution in the southwestern Indian Ocean. Meridional heat transport is strongly concentrated within the upper ocean and closely follows the velocity structure of the current, indicating that variations in current strength directly modulate thermal energy transport. Analysis of wind stress curl reveals only a weak relationship with transport variability ($r \approx 0.11$), with no significant lagged response or coherent spatial structure, suggesting that local atmospheric forcing plays a minor role in controlling transport fluctuations.

Composite analyses of extreme transport states show that variability is primarily associated with changes in current intensity rather than shifts in position. High-transport periods are characterized by a strengthened and coherent current core, whereas low-transport periods exhibit weakened and

fragmented flow structures. These results indicate that Agulhas Current variability is governed predominantly by intrinsic ocean dynamics, mesoscale instability, and large-scale circulation adjustments rather than direct local wind forcing.

KEYWORDS: Agulhas Current; Western Boundary Current Dynamics; Volume Transport Variability; Ocean Heat Transport; Interannual Variability; Indian Ocean Dipole; ENSO; Wind Stress Curl.

1. Introduction

Western boundary currents are among the most energetic components of the global ocean circulation and play a fundamental role in the redistribution of heat, salt, freshwater, and momentum between tropical and high-latitude oceans. As the western boundary current of the South Indian Ocean subtropical gyre, the Agulhas Current represents one of the strongest current systems in the world ocean, transporting warm and saline tropical waters poleward along the southeastern coast of Africa. Owing to its large transport, intense mesoscale variability, and climatic significance, the Agulhas Current exerts a profound influence on regional circulation, air–sea interactions, marine ecosystems, and global climate variability.

The Agulhas Current system forms a critical component of the inter-ocean exchange between the Indian and Atlantic Oceans. After flowing southward along the African continental margin, the current undergoes a dramatic retroflection south of Africa, where most of its transport returns eastward into the Indian Ocean as the Agulhas Return Current. However, a fraction of the flow escapes into the South Atlantic through a process known as Agulhas leakage. This leakage occurs through the shedding of Agulhas Rings, eddies, and filaments that transport substantial quantities of heat and salt from the Indian Ocean into the Atlantic Ocean. Consequently, the Agulhas system constitutes a major choke point of the global overturning circulation and plays a critical role in regulating the upper limb of the Atlantic Meridional Overturning Circulation (AMOC) (Biastoch et al., 2009; Beal et al., 2011). Variations in Agulhas leakage have been linked to changes in Atlantic stratification, salinity budgets, and long-term AMOC variability, emphasizing the broader climatic significance of the Agulhas system. Recent studies further suggest that changes in Southern Hemisphere wind systems may influence leakage variability and inter-basin exchange, thereby affecting large-scale climate processes.

The dynamical structure of the Agulhas Current is characterized by strong western boundary intensification, energetic mesoscale variability, and complex interactions between atmospheric and oceanic processes. Previous observational and modeling investigations have demonstrated that the current exhibits substantial variability over a wide range of temporal and spatial scales. Mesoscale meanders, Natal Pulses, eddy interactions, and upstream

variability originating from the Mozambique Channel and East Madagascar Current contribute significantly to fluctuations in transport and current structure. Furthermore, the Agulhas retroflection region is recognized as one of the most dynamically active regions of the global ocean, where nonlinear instabilities generate Agulhas Rings that subsequently transport Indian Ocean waters into the South Atlantic. Recent syntheses highlight the importance of mesoscale and submesoscale processes in regulating leakage variability, ocean mixing, and inter-ocean exchange within the greater Agulhas system.

Although the Agulhas Current has been extensively studied, important uncertainties remain regarding the mechanisms governing its transport variability. The large-scale circulation is fundamentally linked to wind-driven subtropical gyre dynamics and western boundary intensification theory. However, the extent to which local atmospheric forcing directly influences transport fluctuations remains unclear. Wind stress curl regulates Sverdrup transport and large-scale gyre circulation, yet several studies indicate that western boundary currents may respond more strongly to basin-scale pressure gradients, remote forcing, and intrinsic ocean variability than to local atmospheric forcing. In addition, mesoscale eddies and nonlinear ocean dynamics may modify or obscure the direct response of the current to atmospheric variability, complicating the interpretation of transport fluctuations.

Large-scale climate modes provide an additional source of variability. The El Niño–Southern Oscillation (ENSO) and the Indian Ocean Dipole (IOD) influence atmospheric circulation, wind fields, and oceanic pressure gradients throughout the Indian Ocean basin. Through these mechanisms, climate modes can affect upper-ocean thermal structure, circulation pathways, and western boundary current dynamics. Moreover, variability associated with the Southern Annular Mode (SAM) and poleward shifts of the Southern Hemisphere westerlies has been linked to changes in Agulhas leakage and inter-ocean exchange. Numerical and observational studies suggest that strengthening westerlies may enhance leakage transport and modify retroflection dynamics, thereby influencing the transfer of heat and salt into the Atlantic Ocean (Biastoch et al., 2009; Beal et al., 2011).

The climatic importance of the Agulhas Current extends beyond volume transport alone. As a major conduit for poleward heat transport in the southwestern Indian Ocean, the current contributes substantially to the redistribution of thermal energy and influences regional weather and climate. Variability in heat transport affects upper-ocean heat storage, air–sea heat exchange, and downstream thermal conditions in both the Indian and Atlantic Oceans. Consequently, understanding the variability of heat transport is essential for evaluating the role of the Agulhas system in regional climate regulation and global ocean heat redistribution.

Despite significant advances in understanding Agulhas dynamics, relatively few studies have simultaneously examined current structure, volume transport variability, heat transport variability, climate-mode influences, and atmospheric forcing within a unified framework. Consequently, the relative contributions of local wind forcing, large-scale climate variability, and internal ocean dynamics to Agulhas transport fluctuations remain incompletely understood. Addressing these uncertainties is particularly important given the role of the Agulhas system in inter-basin exchange and its potential influence on future climate variability.

The present study investigates the structure and variability of the Agulhas Current using a comprehensive Eulerian framework based on ocean reanalysis and atmospheric datasets. Specifically, the objectives are to: (1) characterize the mean circulation and transport structure of the Agulhas Current; (2) quantify the spatial and temporal variability of volume and heat transport; (3) examine the influence of large-scale climate modes, including ENSO and the Indian Ocean Dipole, on transport variability; and (4) assess the role of local wind stress curl forcing in modulating current strength. We hypothesize that (i) transport variability is governed primarily by intrinsic ocean dynamics rather than direct local wind forcing, (ii) heat transport variability is closely linked to fluctuations in current intensity, and (iii) large-scale climate modes influence transport indirectly through basin-scale circulation adjustments. By integrating circulation diagnostics, transport estimates, climate indices, and atmospheric forcing analyses, this study aims to improve understanding of the mechanisms governing Agulhas Current variability and its role within the broader climate system.

2. Data and Methodology

2.1 Study Area

The Agulhas Current system is located in the southwestern Indian Ocean and forms the western boundary current of the South Indian Ocean subtropical gyre. Originating from the confluence of the Mozambique Channel flow and the East Madagascar Current, the Agulhas Current flows southwestward along the southeastern coast of Africa before undergoing retroflection south of Africa and partially returning to the Indian Ocean as the Agulhas Return Current (Lutjeharms, 2006; Beal et al., 2011). The study domain encompasses the main Agulhas Current pathway, retroflection region, and adjacent southwestern Indian Ocean (Fig. 2). A transport section was defined approximately normal to the mean current axis to capture the principal volume and heat transport associated with the current system.

2.2 Oceanographic and Atmospheric Datasets

2.2.1 Ocean Reanalysis Data

Ocean circulation and hydrographic fields were obtained from the Simple Ocean Data Assimilation Version 3.15.2 (SODA3) reanalysis (Carton et al., 2018). SODA3 is based on the Modular Ocean Model version 5 (MOM5) and assimilates a wide range of ocean observations, including satellite altimetry, sea-surface temperature, Argo profiles, expendable bathythermographs (XBTs), and moored observations (https://apdrc.soest.hawaii.edu/).

Monthly mean fields spanning 1980–2022 were utilized in this study. The native model resolution is approximately 0.25° with 50 vertical levels extending from the surface to the deep ocean. Variables used include:

Zonal velocity (u)

Meridional velocity (v)

Potential temperature (T)

These fields were used to estimate mean circulation structure, volume transport, and meridional heat transport.

2.2.2 Atmospheric Reanalysis Data

Atmospheric forcing fields were obtained from the ERA5 reanalysis (https://cds.climate.copernicus.eu/) produced by the European Centre for Medium-Range Weather Forecasts (ECMWF) (Hersbach et al., 2020).

Monthly mean:

10-m zonal wind (U10)

10-m meridional wind (V10)

were used to calculate wind stress and wind stress curl. ERA5 provides a horizontal resolution of approximately 0.25° and is widely used for investigations of air–sea interaction and ocean circulation forcing.

2.2.3 Climate Indices

To investigate large-scale climate influences, monthly Niño-3.4 and Dipole Mode Index (DMI) data were obtained from the National Oceanic and Atmospheric Administration (NOAA).

The Niño-3.4 index was used as a measure of El Niño–Southern Oscillation (ENSO) variability (Trenberth, 1997), while DMI was used to represent the Indian Ocean Dipole (Saji et al., 1999).

2.3 Eulerian Transport Framework

Transport calculations were performed using an Eulerian framework in which ocean properties were evaluated across a fixed transect intersecting the Agulhas Current. Similar

approaches have been widely applied in western boundary current studies (Beal and Elipot, 2016).

Velocity fields were interpolated onto the transport section and projected onto the local section-normal direction. The total volume transport Q was calculated as:

$$T = \int\int v_n \, dz \, ds$$

where $v_n$represents the velocity normal to the section, dz is vertical layer thickness, and ds is horizontal distance along the section. Transport values were expressed in Sverdrups (Sv).

2.4 Heat Transport Calculation

Meridional heat transport was calculated following standard ocean heat transport formulations (Ganachaud and Wunsch, 2003):

$$Q = \rho C_p \int \int v_n T \, dz \, ds$$

where ρ is seawater density (1025 kg m^{-3}), C_p is the specific heat capacity of seawater (3990 J kg^{-1} $°C^{-1}$), v_n is section-normal velocity and T is ocean temperature.

Temperature fields were interpolated onto the velocity grid prior to integration. Heat transport estimates were expressed in petawatts (PW).

2.5 Wind Stress Curl Analysis

Surface wind stress was estimated using the bulk aerodynamic formulation (Large and Pond, 1981):

$$\tau_x = \rho_{air} C_d U u$$

$$\tau_y = \rho_{air} C_d U v$$

Where ρ_{air} is air density, C_d is the drag coefficient, U is wind speed magnitude, and u and v are zonal and meridional wind components.

Wind stress curl was then computed as:

$$\nabla \times \tau = \frac{\partial \tau_y}{\partial x} - \frac{\partial \tau_x}{\partial y}$$

Regional averages were used to assess the relationship between atmospheric forcing and transport variability.

2.6 Time Series Processing

Monthly transport and wind-stress-curl time series were standardized to a common temporal framework.

Seasonal variability was removed using climatological monthly means:

$$X' = X - \bar{X}_{month}$$

where X'represents the anomaly field, $\bar{X}_{month}$ denotes the climatological monthly mean..

Linear trends were removed prior to variability analysis to isolate interannual and longer-timescale fluctuations.

2.7 Spectral Analysis

2.7.1. Meridional Volume Transport

The meridional volume transport across the zonal section at 34°S was calculated by integrating the meridional velocity component, v, over the cross-sectional area. In continuous form, the transport is given by

$$T(t) = \int_{x_1}^{x_2} \int_{z_b}^{z_s} v(x,z,t) dz dx$$

where T(t) is the volume transport (m^3/s), v is the meridional velocity (m/s), x denotes the zonal distance along the section, and z represents depth. The limits x_1 and x_2 correspond to 20°E and 40°E, respectively, while z_s and z_b denote the surface and bottom boundaries.

For the discretized model grid, the above transport equation was approximated as

$$T(t) \approx \sum_{i=1}^{N_z} \sum_{j=1}^{N_x} v_{ij}(t) \Delta z_i \Delta x_j$$

where N_z and N_x are the number of depth levels and longitude grid points, respectively; v_{ij} is the meridional velocity at grid cell (i,j); Δz_i is the vertical layer thickness; and Δx_j is the zonal grid spacing.

The zonal grid spacing was calculated using the spherical Earth approximation (Stewart, 2008),

$$\Delta x_j = R cos(\emptyset) \Delta \lambda_j$$

where $R=6.371\times10^6$ m is Earth's radius, ϕ is the latitude of the section (34°S), and $\Delta\lambda_j$ is the longitudinal grid spacing in radians.

The resulting transport was converted to Sverdrups (S_v) according to $T_{S_v} = \frac{T}{10^6}$ where 1 S_v = 10^6 m^3/s.

To investigate the dominant temporal variability of the transport, the transport time series was linearly detrended prior to spectral analysis. The power spectral density (PSD) was estimated using both Welch and multitaper methods.

For a stationary time series x(t), the PSD is defined as the Fourier transform of the autocovariance function (Priestley, 1981),

$$S(f) = \int_{-\infty}^{\infty} R(\tau) e^{-i2\pi f t} d\tau$$

where $R(\tau)$ is the autocovariance function, f is frequency, and τ is the time lag.

2.7.2. Welch Spectrum

The Welch estimator computes the PSD by averaging periodograms obtained from overlapping data segments (Welch, 1967):

$$S_{MT}(f) = \frac{1}{K}\sum_{k=1}^{K} I_k(f)$$

where K is the number of segments and $I_k(f)$ is the periodogram of the k-th segment. In this study, a segment length of 128 months with 50% overlap was used.

2.7.3. Multitaper Spectrum

The multitaper method estimates the PSD using multiple orthogonal tapers (Thomson, 1982):

$$S_{MT}(f) = \frac{1}{K}\sum_{k=1}^{K} w_k(f)\, I_k(f)$$

where $I_k(f)$ is the tapered spectral estimate obtained using the k-th discrete prolate spheroidal sequence (DPSS) taper, and $w_k(f)$ represents the adaptive weighting coefficients. This method reduces spectral leakage and improves the statistical stability of spectral estimates, particularly at low frequencies.

Spectra were computed assuming a monthly sampling interval (Δt=1 month, corresponding to a sampling frequency f_s =1 cycle month−1). Results are presented on logarithmic frequency–power axes to facilitate identification of dominant modes of variability across a wide range of timescales.

2.8 Correlation and Lag Analysis

Pearson correlation coefficients were calculated to quantify relationships among:

- Agulhas transport
- Wind stress curl
- Niño-3.4
- DMI

Lag correlations were computed over ±12 months to identify delayed responses between atmospheric forcing and transport variability.

Statistical significance was evaluated using Student's t-test at the 95% confidence level..

2.9 Composite Analysis

To identify circulation characteristics associated with extreme transport conditions, transport anomalies were categorized into:

- High-transport years (> +1 standard deviation)
- Low-transport years (< −1 standard deviation)

Composite velocity and transport fields were calculated separately for each category. Statistical significance of composite differences was assessed using a two-tailed Student's t-test ($p < 0.05$).

2.10 Spatial Correlation Analysis

Spatial correlations between wind stress curl anomalies and transport variability were calculated at each grid point across the study domain. This analysis provides a geographical assessment of the extent to which local atmospheric forcing contributes to Agulhas Current transport variability and identifies regions exhibiting statistically significant coupling.

3. Results

3.1 Mean Circulation Structure of the Agulhas Current

The mean circulation pattern of the Agulhas Current is presented in Figure 3, while the corresponding vertical structure is shown in Figure 4. The current forms a narrow and intense western boundary jet along the southeastern coast of Africa, characterized by strong poleward flow concentrated adjacent to the continental slope. The current exhibits pronounced western boundary intensification, consistent with the classical dynamics of subtropical gyre circulation (Lutjeharms, 2006; Beal et al., 2011).

The vertical section (Figure 4) reveals a surface-intensified current core extending to depths of approximately 800–1000 m. The strongest velocities occur within the upper ocean and gradually weaken with depth, although a coherent subsurface signal remains evident throughout the upper thermocline. The confinement of high velocities near the continental margin indicates that the majority of transport is concentrated within a relatively narrow boundary current corridor.

Together, Figures 3 and 4 demonstrate that the Agulhas Current functions as a vertically coherent western boundary current capable of transporting substantial volumes of water, heat, and salt toward the southern Indian Ocean.

3.2 Seasonal Variability of Transport

The seasonal cycle of Agulhas Current transport is shown in Figure 5. Monthly climatological transport exhibits relatively small variations throughout the annual cycle, with only modest departures from the long-term mean.

The weak amplitude of the seasonal cycle indicates that seasonal forcing contributes only a limited fraction of the total transport variance. No persistent seasonal maximum or minimum is observed, suggesting that transport variability is dominated by processes operating on interannual and longer timescales rather than by direct seasonal forcing.

These results are consistent with previous studies that identified weak seasonality and strong mesoscale variability as characteristic features of the Agulhas Current system (Beal and Elipot, 2016).

3.3 Spectral and Interannual Variability

The power spectrum of Agulhas Current transport anomalies is shown in Figure 6. Spectral energy is concentrated primarily at low frequencies, indicating that transport variability is dominated by interannual and longer-timescale fluctuations. The absence of a strong annual peak further confirms the weak seasonal modulation identified in Figure 5.

Interannual variability is illustrated in Figure 7a. The transport record exhibits alternating periods of enhanced and reduced transport that persist over several years, indicating the presence of substantial low-frequency variability. These fluctuations occur without a systematic long-term trend and reflect the dynamically variable nature of the Agulhas system.

The predominance of low-frequency variability suggests that transport fluctuations are associated with large-scale oceanic adjustments and internal dynamical processes rather than high-frequency atmospheric forcing.

3.4 Relationship with Large-Scale Climate Modes

Figure 7b compares Agulhas Current transport variability with the Niño-3.4 and Dipole Mode Index (DMI) time series representing ENSO and Indian Ocean Dipole variability, respectively.

Periods of enhanced transport occasionally coincide with phases of ENSO and IOD variability. However, the correspondence is not consistent throughout the record. Some transport anomalies occur during significant climate events, whereas others arise independently of the climate indices.

The episodic nature of these relationships suggests that large-scale climate modes may influence Agulhas transport indirectly through basin-scale circulation adjustments, but they do not represent the primary source of variability. Instead, transport fluctuations likely arise from the combined influence of remote climatic forcing and intrinsic ocean dynamics (Biastoch et al., 2009; Beal et al., 2011).

3.5 Spatial and Vertical Distribution of Heat Transport

The mean meridional heat transport associated with the Agulhas Current is shown in Figure 8. Substantial poleward heat transport occurs along the western boundary of the southwestern Indian Ocean, confirming the role of the Agulhas Current as a major conduit for thermal energy redistribution.

Spatial variability in heat transport closely follows changes in current intensity and structure. Reduced transport near the southern boundary reflects the influence of the Agulhas retroflection, which redirects part of the flow eastward into the Indian Ocean and modulates downstream heat export.

The vertical distribution of heat transport is presented in Figure 9. Heat transport is strongly surface-intensified, with the majority of the poleward heat flux confined to the upper few hundred metres of the water column. Heat transport decreases rapidly with depth owing to the combined reduction in current velocity and temperature gradients.

The close correspondence between Figures 4 and 9 indicates that the vertical distribution of heat transport is primarily governed by the velocity structure of the current. Consequently, changes in current intensity directly influence the magnitude of poleward heat transport.

3.6 Volume Transport Variability

The temporal evolution of Agulhas Current volume transport is shown in Figure 10. The current exhibits a mean southward transport of approximately −62.97 Sv, while transport within the current core averages approximately −67.19 Sv. The standard deviation of approximately 20.66 Sv indicates substantial variability around the mean state.

Transport fluctuations occur across a broad range of timescales and include both short-term and interannual variations. Periods of enhanced transport are characterized by strengthening of the current core, whereas weaker transport periods correspond to reduced current intensity.

No statistically significant long-term trend is evident over the analysis period, indicating that the Agulhas Current remains approximately stationary in its mean transport characteristics despite substantial temporal variability.

3.7 Influence of Wind Stress Curl

The relationship between local atmospheric forcing and Agulhas transport variability is examined in Figure 11. The correlation between transport anomalies and wind stress curl anomalies is weak ($r \approx 0.11$; $r^2 \approx 0.01$), indicating that local wind forcing explains only a small fraction of the observed transport variability.

Lag-correlation analysis reveals no meaningful delayed response between wind stress curl and transport, with maximum correlation occurring near zero lag. Similarly, spatial correlation patterns exhibit weak and spatially incoherent structures throughout the study region.

These results indicate that local wind stress curl exerts only a minor influence on Agulhas Current transport variability and suggest that transport fluctuations are primarily controlled by large-scale pressure gradients and intrinsic ocean dynamics.

3.8 Composite Analysis and Conceptual Synthesis

Composite velocity anomalies for high- and low-transport states are presented in Figure 12. High-transport conditions are characterized by a strengthened and spatially coherent western boundary current, whereas low-transport states exhibit weaker and more fragmented flow structures.

The difference field highlights statistically significant positive velocity anomalies confined to the Agulhas Current pathway, indicating that transport variability primarily reflects changes in current intensity rather than large-scale displacement of the current axis. The spatial confinement of these anomalies further suggests that variability is generated within the boundary current system itself. The schematic highlights the dominant role of internal ocean dynamics and mesoscale variability in regulating transport fluctuations and inter-basin exchange, while illustrating the broader climatic significance of the Agulhas system through its connection to Atlantic buoyancy forcing and the Atlantic Meridional Overturning Circulation (AMOC) (Beal et al., 2011; Biastoch et al., 2009).

4. Discussion

4.1 Mean Structure and Transport Characteristics of the Agulhas Current

The present analysis confirms that the Agulhas Current is a narrow, energetic western boundary current characterized by strong poleward flow along the southeastern coast of Africa. The mean circulation pattern and vertical structure (Figures 3 and 4) reveal a surface-intensified current extending to depths of approximately 800–1000 m, consistent with previous observational and modeling studies (Lutjeharms, 2006; Beal et al., 2011). The confinement of the current core near the continental slope reflects the classical process of western boundary intensification associated with subtropical gyre circulation.

The estimated mean transport of approximately 63 Sv is consistent with reported values from hydrographic observations, current-meter arrays, and numerical simulations, which generally range between 60 and 80 Sv (Beal et al., 2011; Beal and Elipot, 2016). The agreement between the present estimates and previous studies provides confidence in the ability of the reanalysis data to reproduce the large-scale characteristics of the Agulhas Current system.

The observed transport magnitude highlights the importance of the Agulhas Current as a major conduit for the poleward redistribution of mass, heat, and salt in the Indian Ocean. As one of the strongest western boundary currents in the global ocean, the Agulhas Current contributes significantly to regional circulation and inter-ocean exchange processes.

4.2 Dominance of Interannual Variability over Seasonal Forcing

One of the principal findings of this study is the relatively weak seasonal cycle compared with the pronounced interannual variability observed in the transport record (Figures 5–7). Seasonal fluctuations account for only a small proportion of total variance, whereas low-frequency oscillations dominate the transport spectrum.

This behaviour contrasts with several eastern boundary current systems where seasonal wind forcing represents the primary source of variability. In the Agulhas Current system, mesoscale eddies, upstream current variability, and basin-scale oceanic adjustments appear to exert greater control over transport fluctuations than direct seasonal atmospheric forcing.

The predominance of interannual variability is consistent with previous investigations that identified strong low-frequency fluctuations associated with variability in the Mozambique Channel, East Madagascar Current, and Agulhas retroflection dynamics (Lutjeharms, 2006; Beal et al., 2011). These results suggest that transport variability is governed primarily by internal oceanic processes and large-scale circulation adjustments rather than by local seasonal forcing.

4.3 Climate-Mode Influences on Agulhas Transport

The comparison between transport anomalies and climate indices indicates that ENSO and IOD variability may influence the Agulhas system, although the relationships are neither persistent nor statistically robust throughout the analysis period (Figure 7). Periods of enhanced or reduced transport occasionally coincide with major ENSO and IOD events; however, substantial transport anomalies also occur in the absence of pronounced climate forcing.

The weak and intermittent correspondence suggests that large-scale climate modes influence Agulhas transport indirectly through modifications of basin-scale wind fields, thermocline structure, and oceanic pressure gradients rather than through direct forcing mechanisms. Such indirect influences may be transmitted through changes in the subtropical gyre circulation and upstream current systems before affecting the Agulhas Current.

Previous studies have demonstrated that climate variability can modulate Indian Ocean circulation through atmospheric teleconnections and oceanic wave propagation. Nevertheless, the present results indicate that external climate forcing alone is insufficient to explain the observed transport variability. Instead, transport fluctuations likely arise from interactions between climate forcing and intrinsic ocean dynamics, including mesoscale variability and retroflection processes (Biastoch et al., 2009; Beal et al., 2011).

4.4 Heat Transport and Climatic Implications

The Agulhas Current serves as a major pathway for poleward heat transport in the southwestern Indian Ocean. The heat transport distribution (Figures 8 and 9) closely follows the velocity structure of the current, with the majority of thermal energy transport concentrated within the upper ocean where both velocities and temperature gradients are strongest.

The strong correspondence between volume transport and heat transport demonstrates that fluctuations in current intensity directly influence the magnitude of heat redistribution. Consequently, periods of enhanced transport are associated with increased poleward heat flux, whereas weaker current states result in reduced heat transport.

The climatic significance of this relationship extends beyond the Indian Ocean. Through its influence on Agulhas leakage, variability in heat and salt transport can affect the thermohaline properties of waters entering the South Atlantic Ocean. Numerous studies have suggested that changes in Agulhas leakage contribute to variations in Atlantic salinity and buoyancy forcing, potentially influencing the Atlantic Meridional Overturning Circulation (AMOC) on longer timescales (Beal et al., 2011; Biastoch et al., 2015). The present findings therefore reinforce the importance of the Agulhas Current as a key component of the global climate system.

4.5 Wind Stress Curl versus Internal Ocean Dynamics

Perhaps the most important result of this study is the weak relationship between local wind stress curl and Agulhas Current transport variability (Figure 11). The correlation coefficient ($r \approx 0.11$) indicates that local wind forcing explains only a very small fraction of the observed transport variance. Furthermore, lag-correlation analyses reveal no coherent delayed response between wind stress curl and transport fluctuations.

These findings suggest that local atmospheric forcing is not the dominant mechanism governing Agulhas transport variability. Instead, transport fluctuations appear to be controlled primarily by intrinsic ocean dynamics, mesoscale variability, and basin-scale pressure-gradient adjustments. This interpretation is supported by the composite analyses (Figure 12), which demonstrate that transport anomalies are associated mainly with changes in current intensity rather than large-scale shifts in current position.

The weak influence of local wind forcing is consistent with the complex nature of the Agulhas system, where transport variability arises from interactions among upstream source waters, retroflection dynamics, mesoscale eddies, and inter-ocean exchange processes. Variability in the Mozambique Channel, East Madagascar Current, and Agulhas retroflection may therefore exert a stronger influence on transport than local atmospheric forcing.

5. Conclusions

This study examined the structure, variability, and forcing mechanisms of the Agulhas Current using ocean reanalysis and atmospheric datasets within an Eulerian transport framework. By combining analyses of circulation structure, volume transport, heat transport, climate variability, and atmospheric forcing, the study provides a comprehensive assessment of the processes governing variability within one of the world's most energetic western boundary current systems.

The mean circulation is characterized by a narrow, surface-intensified western boundary current flowing poleward along the southeastern coast of Africa, with the current core extending to depths of approximately 800–1000 m. The estimated mean volume transport of approximately 63 Sv confirms the Agulhas Current as one of the strongest western boundary currents in the global ocean and is consistent with previous observational and modeling estimates (Lutjeharms, 2006; Beal et al., 2011; Beal and Elipot, 2016). Transport variability is substantial, with a standard deviation of approximately 21 Sv, reflecting the highly dynamic nature of the Agulhas system.

Temporal analyses indicate that interannual and longer-timescale fluctuations dominate transport variability, whereas seasonal variability contributes only a minor fraction of the total variance. Spectral analyses reveal the predominance of low-frequency variability, suggesting that transport fluctuations are associated primarily with basin-scale circulation adjustments and intrinsic ocean dynamics. Comparisons with the Niño-3.4 and Dipole Mode Index (DMI) indicate episodic correspondence between transport anomalies and large-scale climate variability; however, no persistent or statistically robust relationship was identified. These findings suggest that ENSO and IOD influence the Agulhas system indirectly through large-scale ocean–atmosphere interactions rather than acting as primary drivers of transport variability (Biastoch et al., 2009; Beal et al., 2011).

Heat transport analyses demonstrate that the Agulhas Current serves as a major conduit for poleward heat redistribution in the southwestern Indian Ocean. The majority of heat transport is concentrated within the upper ocean and closely follows the vertical structure of the current. Variations in current strength directly modulate the magnitude of heat transport, emphasizing the importance of transport fluctuations for regional heat budgets and ocean–atmosphere interactions.

A key finding of this study is the weak relationship between local wind stress curl and transport variability. The low correlation coefficient ($r \approx 0.11$) indicates that local atmospheric forcing explains only a small proportion of the observed transport fluctuations.

Composite analyses further reveal that variability is associated primarily with changes in current intensity rather than substantial shifts in current position. Collectively, these results indicate that Agulhas Current variability is governed predominantly by intrinsic ocean dynamics, mesoscale variability, upstream circulation fluctuations, and basin-scale pressure-gradient adjustments rather than by direct local wind forcing. This interpretation is consistent with previous studies emphasizing the importance of mesoscale processes and remote forcing in regulating variability within the greater Agulhas system (Lutjeharms, 2006; Beal et al., 2011).

The findings underscore the climatic significance of the Agulhas Current as a major pathway for the transport of heat and salt between the Indian and Atlantic Oceans. Through its connection to Agulhas leakage, variability within the Agulhas system has the potential to influence Atlantic salinity distributions, buoyancy forcing, and components of the Atlantic Meridional Overturning Circulation (AMOC), thereby linking regional ocean dynamics to broader climate variability (Biastoch et al., 2009; Beal et al., 2011; Biastoch et al., 2015). Future investigations incorporating eddy kinetic energy, sea-surface height variability, Agulhas leakage diagnostics, and Southern Annular Mode influences would further improve understanding of the mechanisms connecting Agulhas Current variability to regional and global climate processes.

Acknowledgements

The authors gratefully acknowledge Andhra University, Visakhapatnam, India, for providing the academic environment, research facilities, and institutional support necessary for carrying out this study. This work is dedicated to Andhra University on the occasion of its centenary celebrations in recognition of its distinguished legacy in education, research, and scientific advancement.

The authors sincerely thank the Asia-Pacific Data Research Center, the European Centre for Medium-Range Weather Forecasts, and the National Oceanic and Atmospheric Administration for providing the SODA and ERA5 datasets, respectively.

Funding: There is no source of funding

Ethics statement: Not Applicable. This study did not involve human participants, human data, human biological material, or live vertebrate animals. The study was based entirely on publicly available oceanographic and atmospheric reanalysis datasets and climate indices.

Consent to Participate: Not Applicable. This study did not involve human participants..

Consent for Publish declaration: Not Applicable. This study does not contain identifiable information or personal data from human participants.

Data Availability Statement: The datasets generated during and/or analysed during the current study are available from the corresponding author on reasonable request.

Authors' contributions

Usha Rani conducted the research, performed data processing and analysis, carried out the mixed-layer heat-budget computations, prepared the figures and visualizations, and wrote the original draft of the manuscript.

K. M. Krishna conceptualized and supervised the study, provided scientific guidance and methodological support, contributed to the interpretation of the results, critically reviewed and edited the manuscript, and supervised the overall research progress.

Competing interests: The authors declare no competing interests.

References:

Anderson, D. L. T., and Gill, A. E. (1975). Spin-up of a stratified ocean, with applications to upwelling. Deep-Sea Research, 22, 583–596.

Barnier, B., Siefridt, L., and Marchesiello, P. (1995). Thermal forcing for a global ocean circulation model using ECMWF data. Tellus A, 47, 545–561.

Beal, L. M., De Ruijter, W. P. M., Biastoch, A., and Zahn, R. (2011). On the role of the Agulhas system in ocean circulation and climate. Nature, 472, 429–436.

Beal, L. M., and Elipot, S. (2016). Broadening not strengthening of the Agulhas Current since the early 1990s. Nature, 540, 570–573.

Biastoch, A., Böning, C. W., and Lutjeharms, J. R. E. (2008). Agulhas leakage dynamics affects decadal variability in Atlantic overturning circulation. Nature, 456, 489–492.

Biastoch, A., Böning, C. W., Schwarzkopf, F. U., and Lutjeharms, J. R. E. (2009). Increase in Agulhas leakage due to poleward shift of Southern Hemisphere westerlies. Nature, 462, 495–498.

Biastoch, A., Durgadoo, J.V., Morrison, A.K., van Sebille, E., Weijer, W., Griffies, S.M., 2015. Atlantic multidecadal oscillation covaries with Agulhas leakage. Nature Communications, 6, 10082.

Boebel, O., Rossby, T., Lutjeharms, J. R. E., Zenk, W., and Barron, C. (2003). Path and variability of the Agulhas Return Current. Deep-Sea Research Part II, 50, 35–56.

Broecker, W. S. (1991). The great ocean conveyor. Oceanography, 4(2), 79–89.

Bryden, H. L., Beal, L. M., and Duncan, L. M. (2005). Structure and transport of the Agulhas Current and its temporal variability. Journal of Oceanography, 61, 479–492.

Buckley, M. W., and Marshall, J. (2016). Observations, inferences, and mechanisms of the Atlantic Meridional Overturning Circulation. Reviews of Geophysics, 54, 5–63.

567 Chassignet, E. P., Hurlburt, H. E., Metzger, E. J., et al. (2007). The HYCOM ocean prediction
568 system. Journal of Marine Systems, 65, 60–83.
569 Chelton, D. B., Schlax, M. G., and Samelson, R. M. (2011). Global observations of nonlinear
570 mesoscale eddies. Progress in Oceanography, 91, 167–216.
571 Cox, M. D. (1985). An eddy-resolving numerical model of the ventilated thermocline. Journal
572 of Physical Oceanography, 15, 1312–1324.
573 de Ruijter, W. P. M., van Leeuwen, P. J., and Lutjeharms, J. R. E. (1999). Generation and
574 evolution of Natal Pulses. Journal of Physical Oceanography, 29, 3043–3055.
575 Dong, S., Sprintall, J., Gille, S. T., and Talley, L. (2009). Southern Ocean mixed-layer depth
576 from Argo float profiles. Journal of Geophysical Research, 113, C06013.
577 Duchez, A., Frajka-Williams, E., Castro, N., et al. (2016). Drivers of exceptionally cold North
578 Atlantic Ocean temperatures and their link to the 2015 European heat wave. Environmental
579 Research Letters, 11, 074004.
580 Durgadoo, J. V., Loveday, B. R., Reason, C. J. C., Penven, P., and Biastoch, A. (2013).
581 Agulhas leakage predominantly responds to the Southern Hemisphere westerlies. Journal of
582 Physical Oceanography, 43, 2113–2131.
583 Emery, W.J., Thomson, R.E., 2001. Data Analysis Methods in Physical Oceanography, 2nd
584 ed. Elsevier Science, Amsterdam, Netherlands, 638 pp.
585 Fairall, C. W., Bradley, E. F., Hare, J. E., et al. (2003). Bulk parameterization of air–sea
586 fluxes. Journal of Climate, 16, 571–591.
587 Ferrari, R., and Wunsch, C. (2009). Ocean circulation kinetic energy: Reservoirs, sources,
588 and sinks. Annual Review of Fluid Mechanics, 41, 253–282.
589 Ganachaud, A., Wunsch, C., 2003. Large-scale ocean heat and freshwater transports during
590 the World Ocean Circulation Experiment. Journal of Climate 16 (4), 696–705.
591 Ganachaud, A., and Wunsch, C. (2000). Improved estimates of global ocean circulation, heat
592 transport, and mixing from hydrographic data. Nature, 408, 453–457.
593 Gill, A. E. (1982). Atmosphere–Ocean Dynamics. Academic Press.
594 Gordon, A. L. (1986). Interocean exchange of thermocline water. Journal of Geophysical
595 Research, 91, 5037–5046.
596 Hersbach, H., Bell, B., Berrisford, P., Hirahara, S., Horányi, A., Muñoz-Sabater, J., Nicolas,
597 J., Peubey, C., Radu, R., Schepers, D., Simmons, A., Soci, C., Abdalla, S., Abellan, X.,
598 Balsamo, G., Bechtold, P., Biavati, G., Bidlot, J., Bonavita, M., De Chiara, G., Dahlgren, P.,
599 Dee, D., Diamantakis, M., Dragani, R., Flemming, J., Forbes, R., Fuentes, M., Geer, A.,
600 Haimberger, L., Healy, S., Hogan, R.J., Hólm, E., Janisková, M., Keeley, S., Laloyaux, P.,

Lopez, P., Lupu, C., Radnoti, G., de Rosnay, P., Rozum, I., Vamborg, F., Villaume, S., Thépaut, J.N., 2020. The ERA5 global reanalysis. Quarterly Journal of the Royal Meteorological Society 146 (730), 1999–2049.

Holton, J. R. (2004). An Introduction to Dynamic Meteorology. Elsevier Academic Press.

IOC, SCOR, and IAPSO (2010). The International Thermodynamic Equation of Seawater – 2010. UNESCO Manuals and Guides No. 56.

Jayne, S. R., and Marotzke, J. (2001). The dynamics of ocean heat transport variability. Reviews of Geophysics, 39, 385–411.

Kelly, K. A., Small, R. J., Samelson, R. M., et al. (2010). Western boundary currents and frontal air–sea interaction. Journal of Climate, 23, 5644–5657.

Large, W.G., Pond, S., 1981. Open ocean momentum flux measurements in moderate to strong winds. Journal of Physical Oceanography 11 (3), 324–336.

Large, W. G., and Yeager, S. G. (2009). The global climatology of an interannually varying air–sea flux dataset. Climate Dynamics, 33, 341–364.

Le Traon, P. Y., Nadal, F., and Ducet, N. (1998). An improved mapping method of multisatellite altimeter data. Journal of Atmospheric and Oceanic Technology, 15, 522–534.

Le Bars, D., van Sebille, E., Durgadoo, J.V., et al., 2022. Robust estimates for the decadal evolution of Agulhas leakage from the 1960s to the 2010s. Communications Earth & Environment, 3, 318.

Lutjeharms, J.R.E., 2006. The Agulhas Current. Springer-Verlag, Berlin Heidelberg, Germany, 330 pp.

Lutjeharms, J. R. E., and Roberts, H. R. (1988). The Natal Pulse: An extreme transient on the Agulhas Current. Journal of Geophysical Research, 93, 631–645.

Marshall, J., and Speer, K. (2012). Closure of the meridional overturning circulation through Southern Ocean upwelling. Nature Geoscience, 5, 171–180.

McDonagh, E. L., Bryden, H. L., King, B. A., et al. (2015). Continuous estimate of Atlantic Ocean heat transport at 26.5°N. Journal of Climate, 28, 888–908.

Moore, J. K., and Abbott, M. R. (2000). Phytoplankton chlorophyll distributions and primary production in the Southern Ocean. Journal of Geophysical Research, 105, 28709–28722.

Munk, W. H. (1950). On the wind-driven ocean circulation. Journal of Meteorology, 7, 79–93.

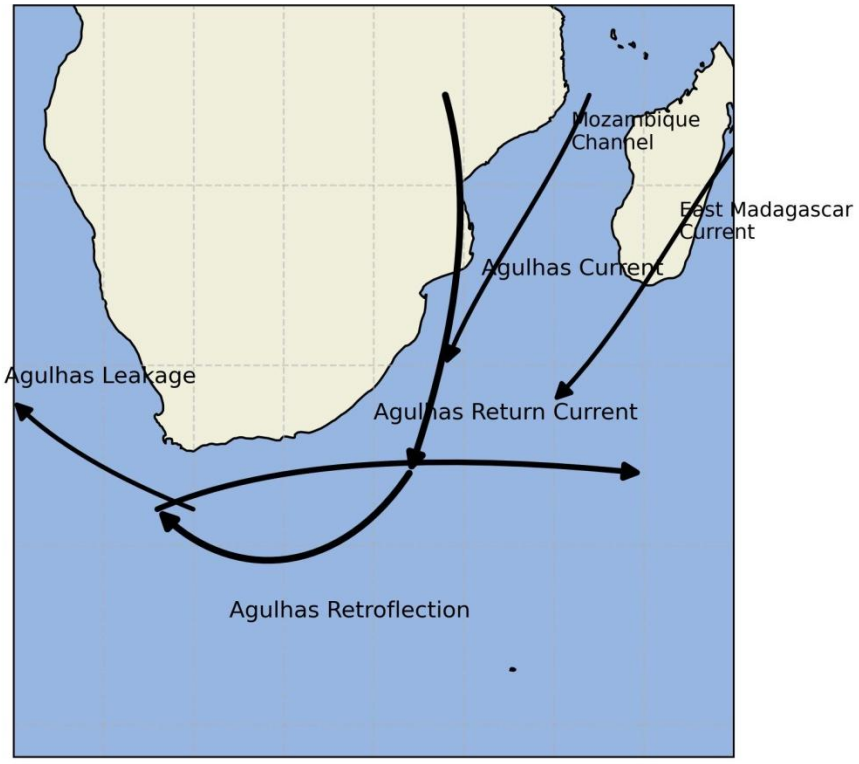
Peeters, F. J. C., Acheson, R., Brummer, G.-J. A., et al. (2004). Vigorous exchange between the Indian and Atlantic Oceans at the end of the past five glacial periods. Nature, 430, 661–665.

635 Penduff, T., Juza, M., Barnier, B., et al. (2010). Sea level expression of intrinsic and forced
636 ocean variabilities. Journal of Climate, 24, 5652–5670.
637 Priestley, M.B., 1981. Spectral Analysis and Time Series. Academic Press, London.
638 Qiu, B. (2002). Large-scale variability in the midlatitude subtropical and subpolar North
639 Pacific Ocean. Journal of Physical Oceanography, 32, 353–375.
640 Rahmstorf, S. (2002). Ocean circulation and climate during the past 120,000 years. Nature,
641 419, 207–214.
642 Reason, C. J. C. (2001). Evidence for the influence of the Agulhas Current on regional
643 atmospheric circulation patterns. Journal of Climate, 14, 2769–2778.
644 Richardson, P. L. (2007). Agulhas leakage into the Atlantic estimated with subsurface floats
645 and surface drifters. Deep-Sea Research Part I, 54, 1361–1389.
646 Roemmich, D., and Gilson, J. (2009). The 2004–2008 mean and annual cycle of temperature,
647 salinity, and steric height in the global ocean from the Argo Program. Progress in
648 Oceanography, 82, 81–100.
649 Sabine, C. L., Feely, R. A., Gruber, N., et al. (2004). The oceanic sink for anthropogenic CO_2.
650 Science, 305, 367–371.
651 Saji, N.H., Goswami, B.N., Vinayachandran, P.N., Yamagata, T., 1999. A dipole mode in the
652 tropical Indian Ocean. Nature 401 (6751), 360–363.
653 Schott, F. A., Xie, S.-P., and McCreary, J. P. (2009). Indian Ocean circulation and climate
654 variability. Reviews of Geophysics, 47, RG1002.
655 Smith, R. L. (1968). Upwelling. Oceanography and Marine Biology Annual Review, 6, 11–
656 46.
657 Speich, S., Blanke, B., and Cai, W. (2007). Atlantic meridional overturning circulation and
658 the Southern Hemisphere supergyre. Geophysical Research Letters, 34, L23614.
659 Stewart Robert H. (2008). Introduction to Physical Oceanography. Texas A&M University.
660 Stommel, H. (1948). The westward intensification of wind-driven ocean currents.
661 Transactions of the American Geophysical Union, 29, 202–206.
662 Swart, S., Speich, S., Ansorge, I. J., et al. (2008). Transport and variability of the Antarctic
663 Circumpolar Current south of Africa. Journal of Geophysical Research, 113, C09014.
664 Talley, L. D., Pickard, G. L., Emery, W. J., and Swift, J. H. (2011). Descriptive Physical
665 Oceanography: An Introduction. Academic Press.
666 Thomson, D.J., 1982. Spectrum estimation and harmonic analysis. Proceedings of the IEEE,
667 70, 1055–1096.

668 Toole, J. M., and Warren, B. A. (1993). A hydrographic section across the subtropical South
669 Indian Ocean. Deep-Sea Research Part I, 40, 1973–2019.
670 Trenberth, K.E., 1997. The definition of El Niño. Bulletin of the American Meteorological
671 Society 78 (12), 2771–2777.
672 Trenberth, K. E., and Caron, J. M. (2001). Estimates of meridional atmosphere and ocean
673 heat transports. Journal of Climate, 14, 3433–3443.
674 van Sebille, E., England, M. H., and Froyland, G. (2010). Origin, dynamics, and evolution of
675 Agulhas rings. Journal of Geophysical Research, 115, C12055.
676 van Sebille, E., Griffies, S. M., Abernathey, R., et al. (2018). Lagrangian ocean analysis:
677 Fundamentals and practices. Ocean Modelling, 121, 49–75.
678 Welch, P.D., 1967. The use of fast Fourier transform for the estimation of power spectra: A
679 method based on time averaging over short, modified periodograms. IEEE Transactions on
680 Audio and Electroacoustics, 15, 70–73.
681 Wu, L., Cai, W., Zhang, L., et al. (2012). Enhanced warming over the global subtropical
682 western boundary currents. Nature Climate Change, 2, 161–166.
683 Wunsch, C., and Ferrari, R. (2004). Vertical mixing, energy, and the general circulation of the
684 oceans. Annual Review of Fluid Mechanics, 36, 281–314.

685 **Figures**

686



687

Figure 1. Location of the Agulhas Current system in the southwestern Indian Ocean. The study domain encompasses the southeastern coast of Africa, the Agulhas Current pathway, the Agulhas Retroflection region, and adjacent portions of the South Atlantic and Indian Oceans. The red line indicates the transport section used for volume and heat transport calculations.

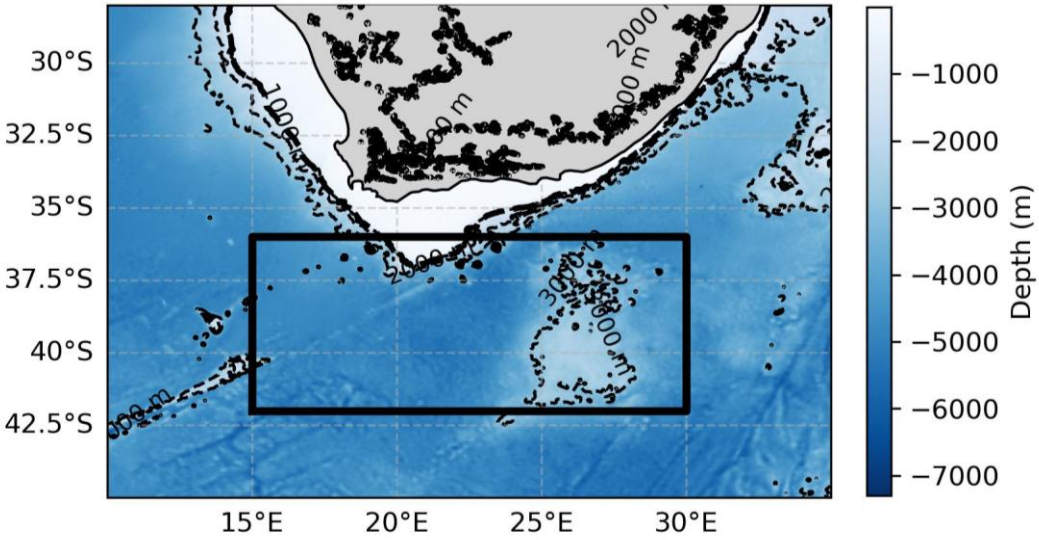


Figure 2. Bathymetry and geographical setting of the study region. Major circulation features of the Agulhas system, Agulhas Retroflection, Agulhas Return Current, and Agulhas leakage pathways. Bathymetry is shaded according to water depth (m).

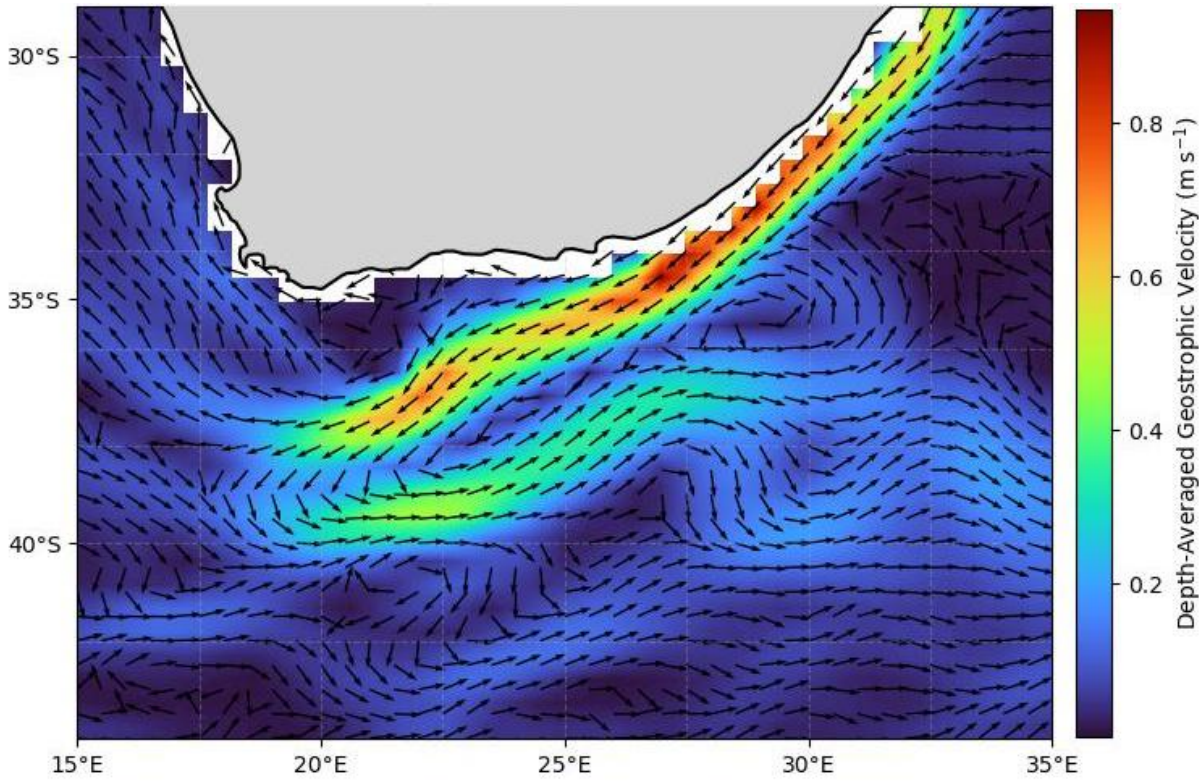


Figure 3. Mean surface circulation of the Agulhas Current derived from SODA reanalysis during the study period. Shading represents current velocity magnitude (m s^{-1}), while vectors indicate current direction. The Agulhas Current appears as a narrow and intense western boundary current flowing southwestward along the southeastern African continental margin before entering the retroflection region south of Africa.

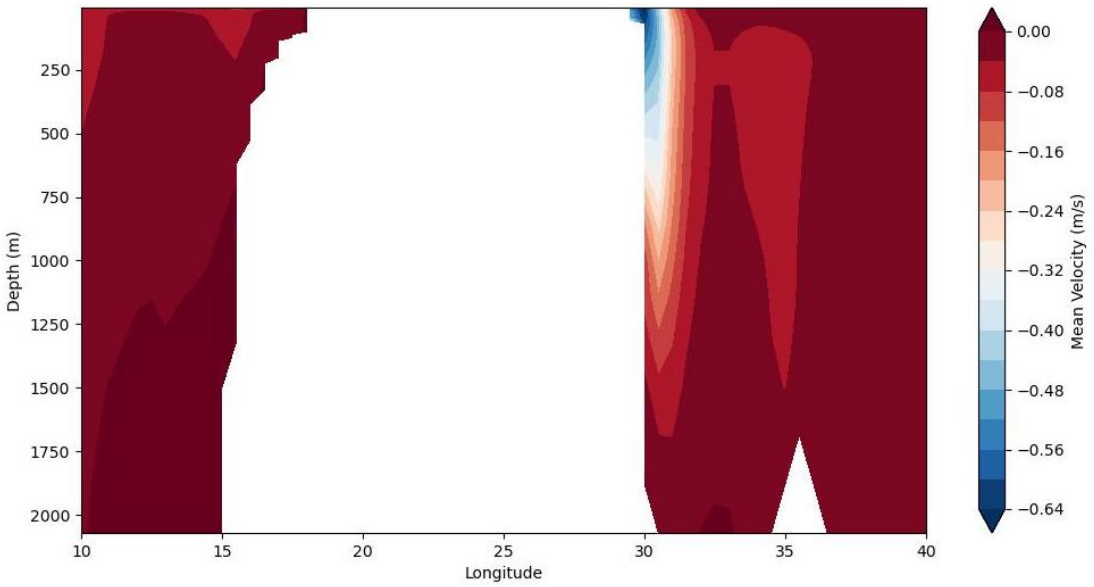


Figure 4. Mean vertical structure of the Agulhas Current along the transport section (~34°S). Shading represents section-normal velocity (m s^{-1}), while contours indicate velocity structure. Positive and negative values denote flow directions relative to the transport section. The figure illustrates the surface-intensified nature of the current and its vertical penetration into the upper ocean.

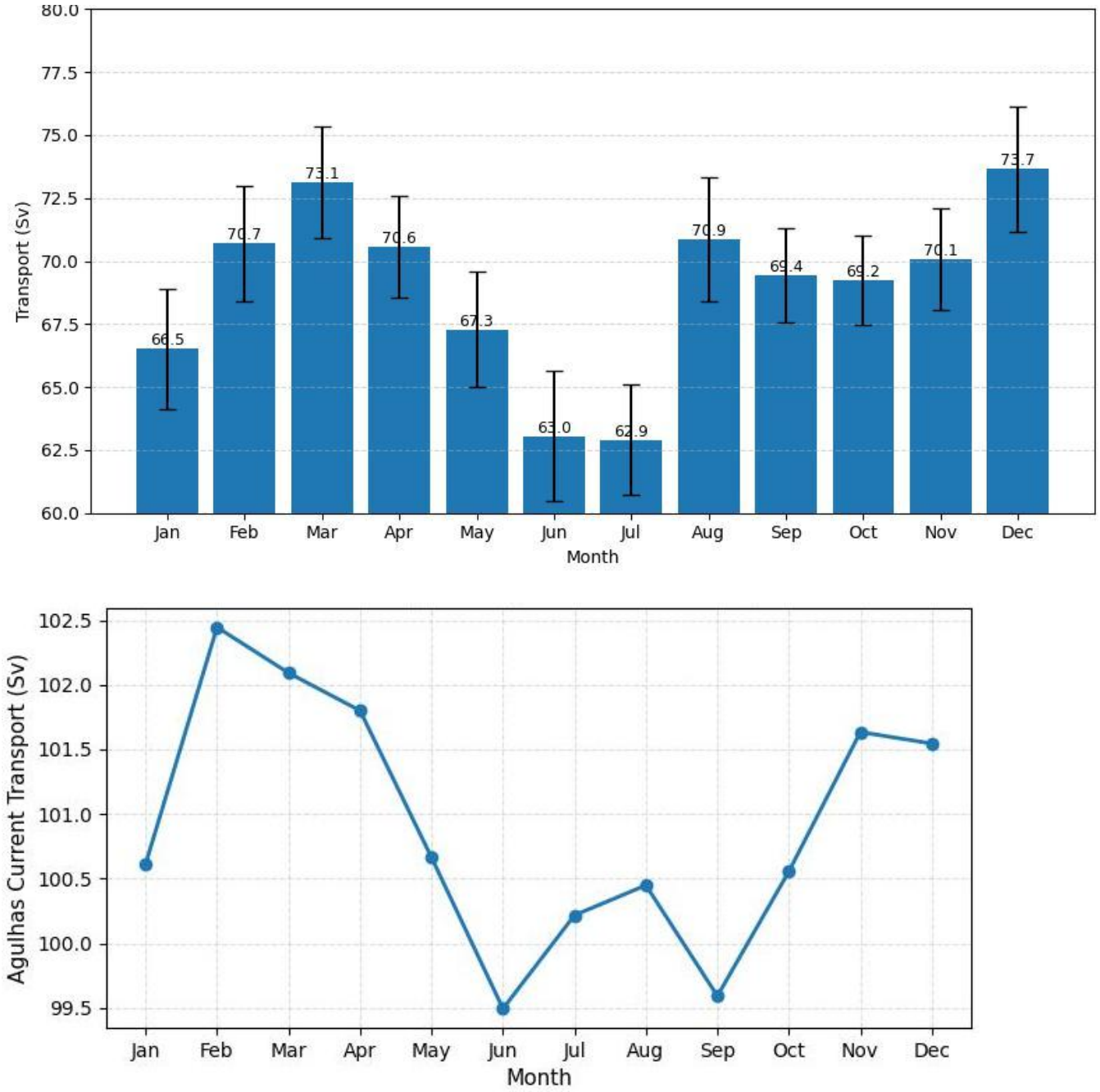


Figure 5. Seasonal cycle of Agulhas Current transport. a, Monthly climatology of volume transport derived from the full study period (Top). b, Monthly transport values shown in an alternative representation to facilitate comparison among months (bottom). Both panels indicate weak seasonal variability, with transport remaining relatively stable throughout the year and exhibiting only minor departures from the annual mean. The results suggest that seasonal forcing plays a limited role in controlling the overall strength of the Agulhas Current.

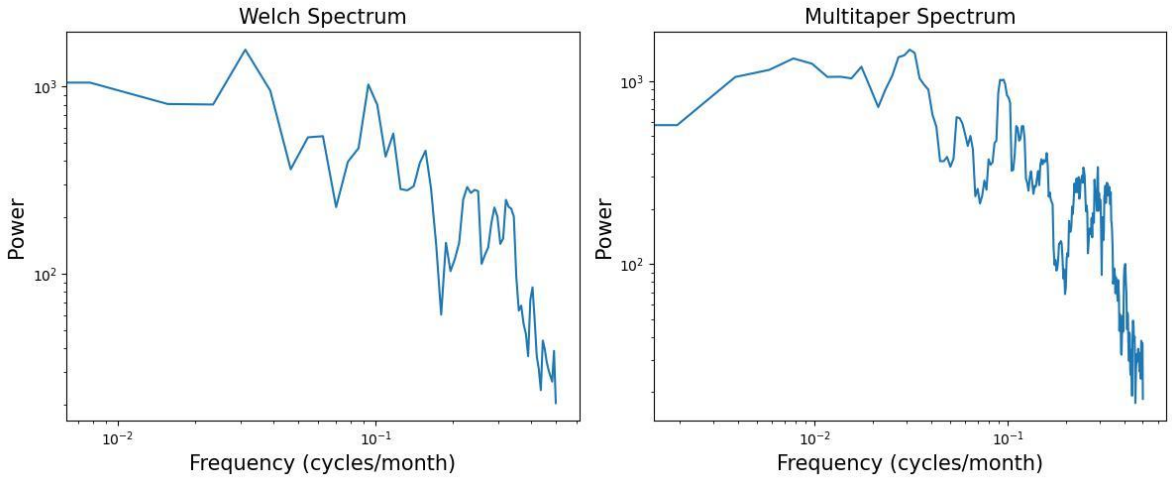
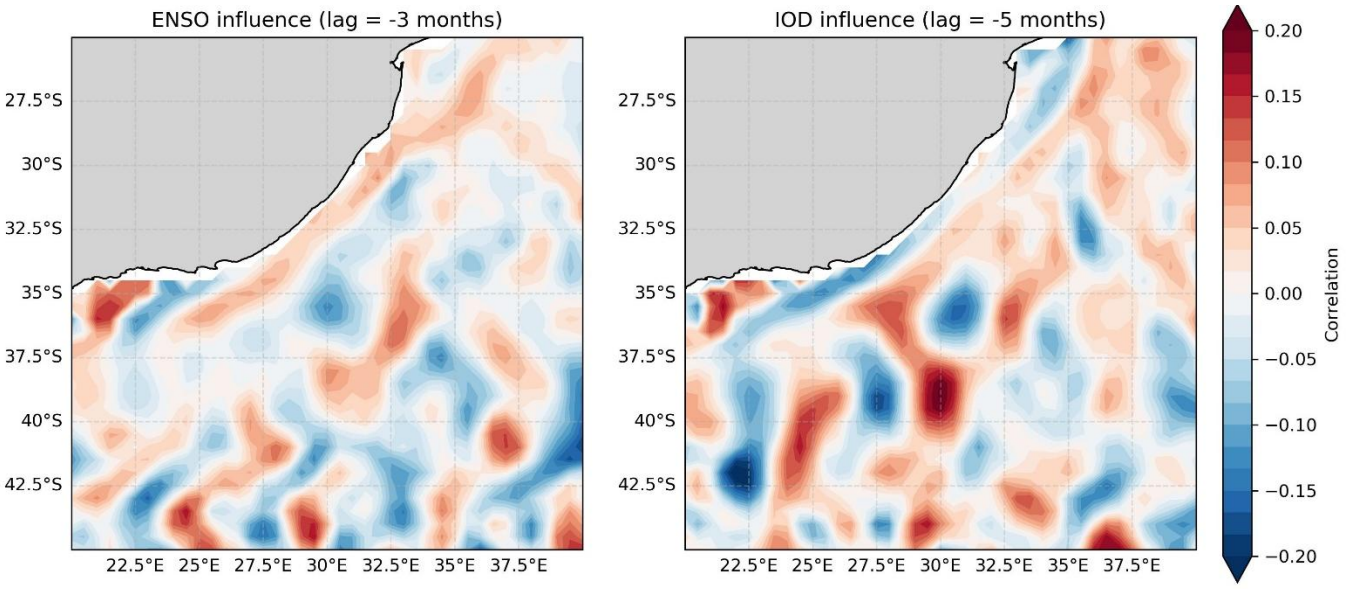


Figure 6. Power spectral density of Agulhas Current transport anomalies.



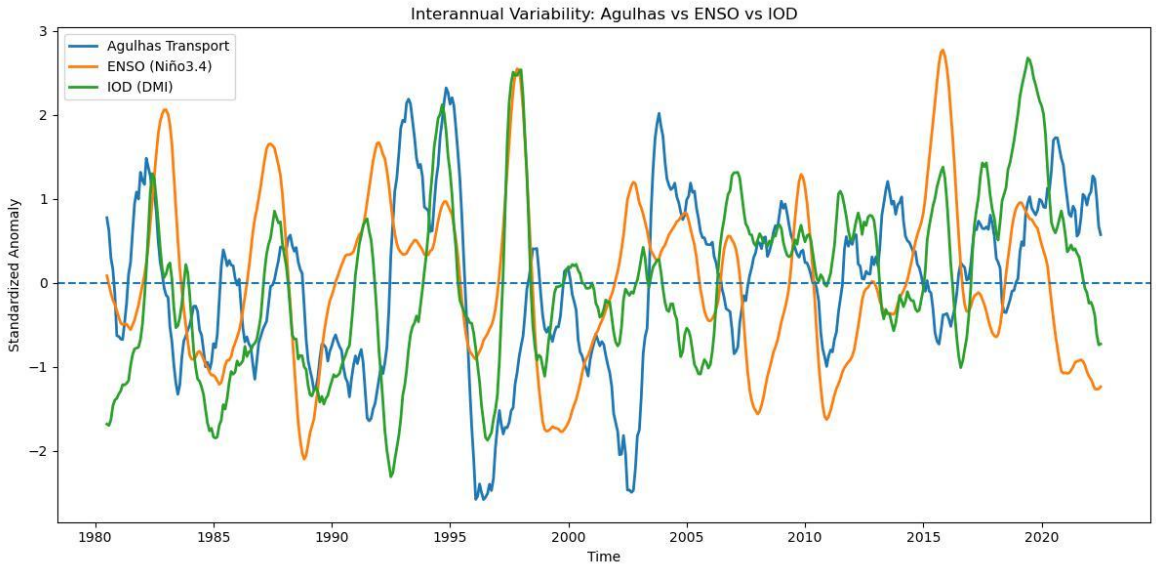


Figure 7. Relationship between Agulhas Current transport variability and large-scale climate modes. (a) Time series of monthly transport anomalies (top). (b) Comparison of standardized Agulhas transport anomalies with the Niño-3.4 index and Dipole Mode Index (DMI) (bottom). Positive and negative phases of ENSO and the Indian Ocean Dipole are indicated to assess potential climate influences on transport variability.

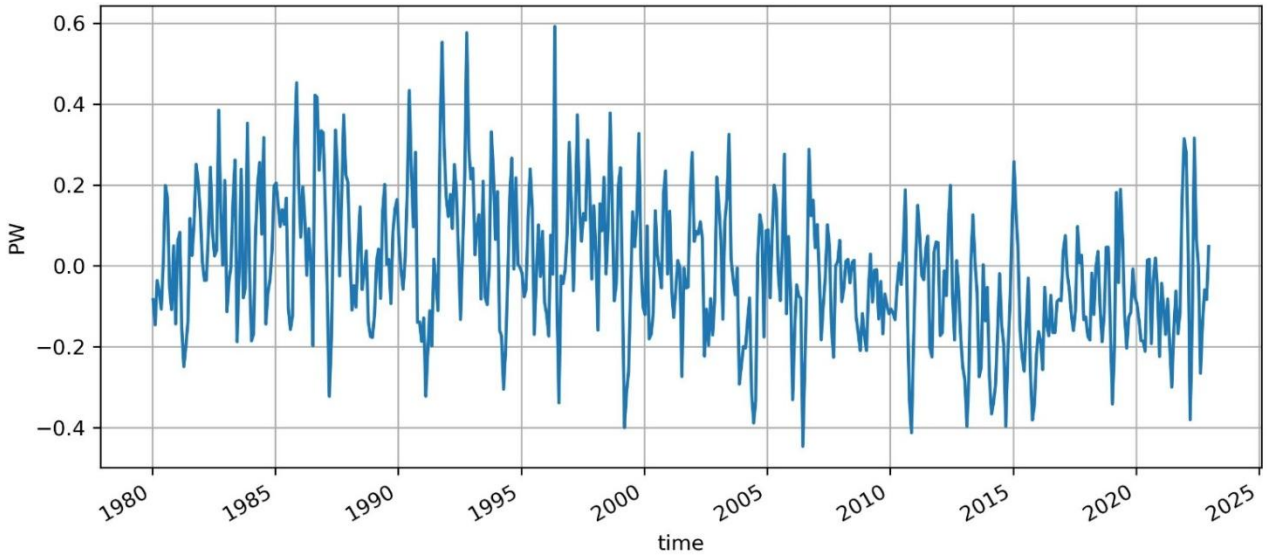


Figure 8. Spatial distribution of mean meridional heat transport associated with the Agulhas Current. Shading represents heat transport magnitude, illustrating the concentration of poleward heat transport within the western boundary current system and its downstream modification near the Agulhas Retroflection region.

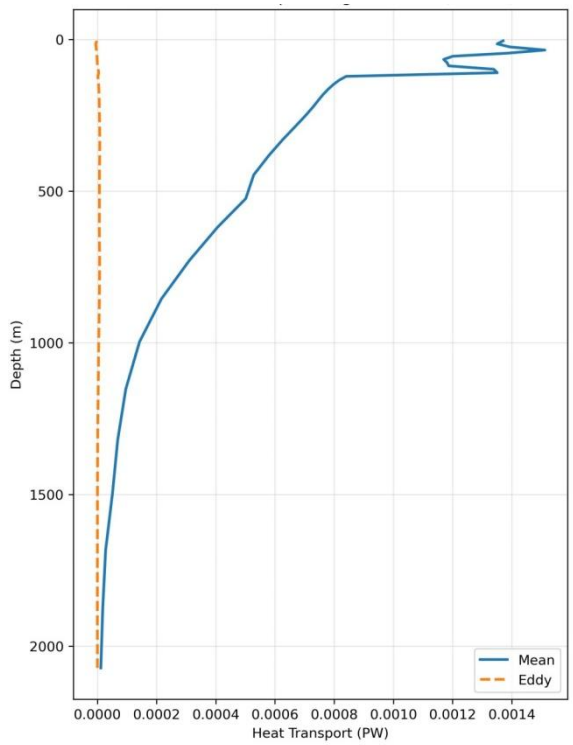


Figure 9. Vertical distribution of meridional heat transport across the Agulhas Current section. Shading indicates heat transport contributions as a function of depth and cross-sectional position. The majority of heat transport is confined to the upper ocean, reflecting the combined influence of strong velocities and elevated temperatures.

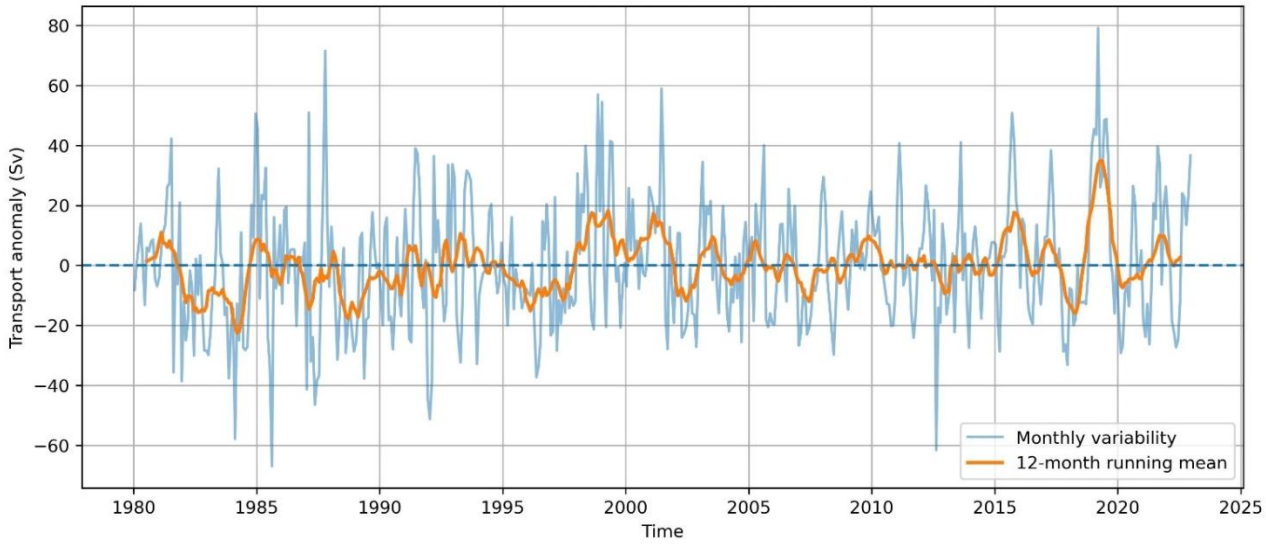


Figure 10. Time series of Agulhas Current volume transport during the study period. The solid line represents monthly transport estimates, while the dashed line indicates the long-term mean transport. Positive and negative anomalies correspond to periods of enhanced and reduced current strength, respectively.

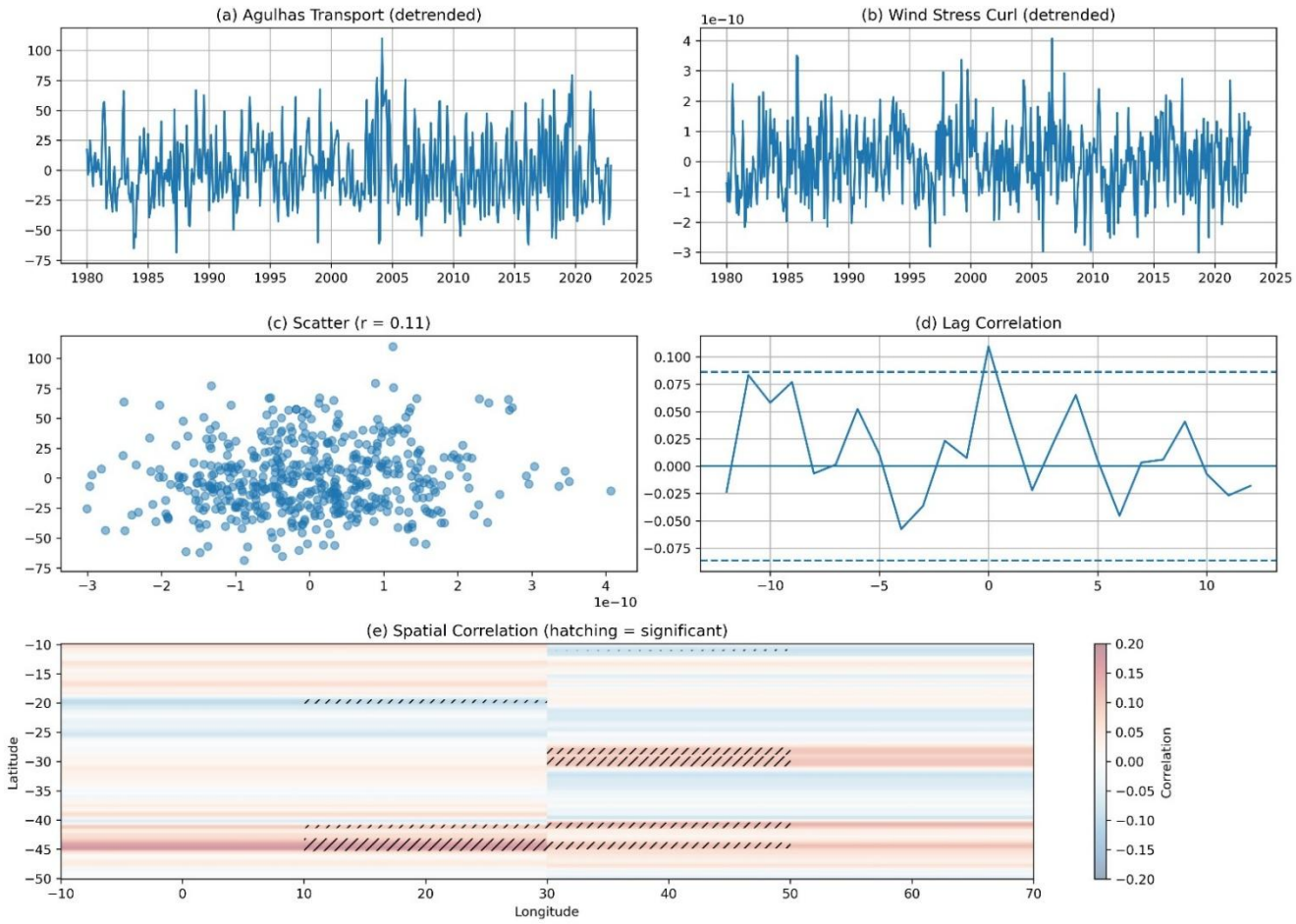


Figure 11. Relationship between Agulhas Current transport variability and wind stress curl. (a) Time series comparison between transport anomalies and regional wind stress curl anomalies. (b) Scatter plot showing the correlation between transport and wind stress curl. (c) Lag-correlation analysis indicating the temporal relationship between atmospheric forcing and transport variability. (d) Spatial correlation between transport anomalies and wind stress curl anomalies across the study region. Stippling indicates statistically significant correlations at the 95% confidence level.

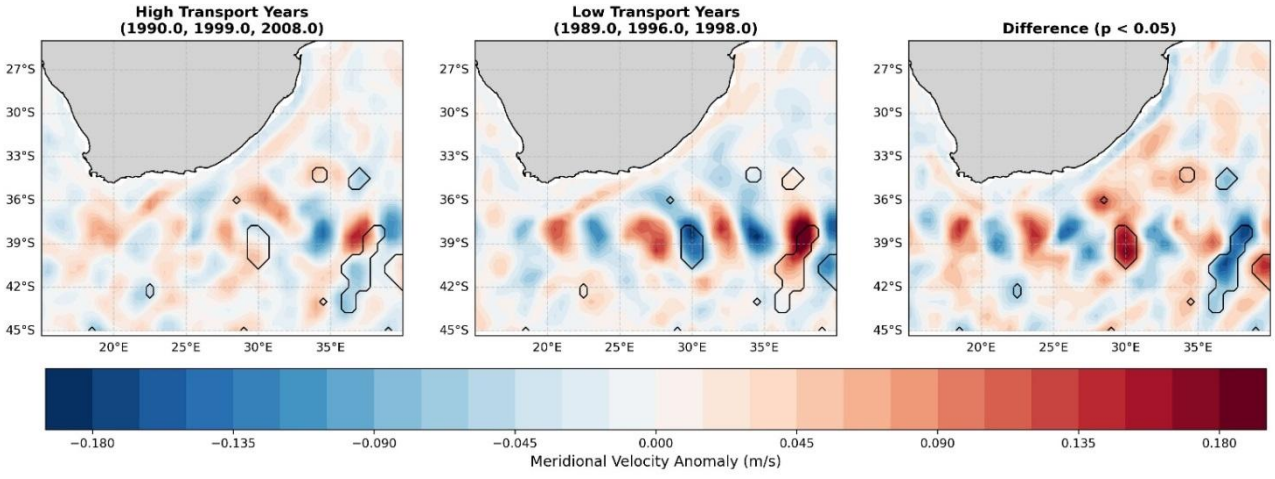


Figure 12. Composite analysis of extreme transport states. (a) Mean circulation during high-transport periods (> +1 standard deviation). (b) Mean circulation during low-transport periods (< −1 standard deviation). (c) Difference between high- and low-transport composites. Shading represents velocity anomalies, and stippling indicates regions where differences are statistically significant at the 95% confidence level. The figure highlights the dominant role of current-intensity changes in generating transport variability.